HHS Public Access

Author manuscript

Langmuir. Author manuscript; available in PMC 2021 August 19.

Published in final edited form as:

Langmuir. 2020 September 22; 36(37): 11034–11043. doi:10.1021/acs.langmuir.0c01894.

Interfacial Electrofabrication of Freestanding Biopolymer Membranes with Distal Electrodes

Piao Hu,
Department of Mechanical Engineering, Catholic University of America, Washington, District of Columbia 20064, United States

Seyed A. Rooholghodos,
Department of Mechanical Engineering, Catholic University of America, Washington, District of Columbia 20064, United States

Le H. Pham,
Department of Mechanical Engineering, Catholic University of America, Washington, District of Columbia 20064, United States

Khanh L. Ly,
Department of Biomedical Engineering, Catholic University of America, Washington, District of Columbia 20064, United States

Xiaolong Luo
Department of Mechanical Engineering, Catholic University of America, Washington, District of Columbia 20064, United States

Abstract

Using electrical signals to guide materials' deposition has a long-standing history in metal coating, microchip fabrication, and the integration of organics with devices. In electrodeposition, however, the conductive materials can be deposited only onto the electrode surfaces. Here, an innovative process is presented to electrofabricate freestanding biopolymer membranes at the interface of electrolytes without any supporting electrodes at the fabrication site. Chitosan, a derivative from the naturally abundant biopolymer chitin, has been broadly explored in electrodeposition for integrating biological entities onto microfabricated devices. It is widely believed that the pH gradients generated at the cathode deprotonate the positively charged chitosan chains into a film on the cathode surface. The interfacial electrofabrication with pH indicators, however, demonstrated that the membrane growth was driven by the instantaneous flow of hydroxyl ions from the ambient alginate solution, rather than the slow propagation of pH gradients from the

Corresponding Author: Xiaolong Luo, Department of Mechanical Engineering, Catholic University of America, Washington, District of Columbia 20064, United States; luox@cua.edu.

Author Contributions

X.L. directed the project; P.H. planned and performed the experiments; S.A.R. participated in the characterization of membrane formation; P.H. analyzed the data; P.H. and X.L. co-wrote the manuscript. All authors participated in experimental design and manuscript discussion.

The authors declare no competing financial interest.

ASSOCIATED CONTENT

Supporting Information

The Supporting Information is available free of charge at https://pubs.acs.org/doi/10.1021/acs.langmuir.0c01894.

cathode surface. This interfacial electrofabrication produces freestanding membrane structures and can be expanded to other materials, which presents a new direction in using electrical signals for manufacturing.

Graphical Abstract

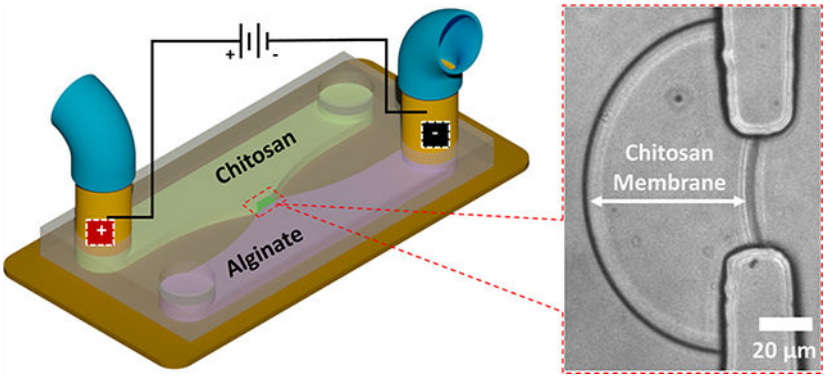

INTRODUCTION

Membranes have been broadly employed in the chemical industry and biological engineering with versatile functions, user and environmental friendliness, and compelling economic benefits as compared to traditional separation techniques.[1] A variety of membrane preparation methods such as solution casting, phase inversion, track-etching, stretching, electrospinning, or sintering have been developed to manufacture membranes for specific applications.[2–6] Among these, the use of electrical signals to guide the deposition of materials in general, and membranes in particular, stands out as a well-established and convenient method. The advantages of the electrodeposition process include time-saving preparation, versatile operation, high uniformity, low energy consumption, and straightforward manipulation over key parameters such as current, voltage, and time.[7–10] Therefore, electrodeposition has been extensively applied in the surface coating of metal and biomaterials, fabrication of electronic chips, and integration of organics with devices.[9–13]

With the rapid development of bioelectronics and biomedical devices, more and more attention has been drawn to the integration of organic biological polymers onto inorganic electronic devices such as biosensors, lab-on-a-chip devices, and bio-microelectromechanical systems (bioMEMS). Diverse bioelectronics and biomedical platforms have been developed aiming at various purposes by converging the biocompatibility, biofunctionality, and mechanical flexibility of biopolymers and the real-time transmission and multiplexing capabilities of electronics.[14–21] Numerous bioelectronics have taken the advantages of the special properties of carbon-based biomaterials,[21–24] including their similarity to biological tissues and versatility in electrical, mechanical, and biofunctional engineering, to minimize the intrinsic differences between biological tissues and man-made electronics.

Chitosan, one of the most adopted biomaterials in biomedical and bioelectronics fields, has been broadly used for applications ranging from tissue engineering to biomedical drug

delivery to bio-microdevices.[25–29] Chitosan is soluble in acidic conditions but becomes insoluble in pH higher than 6.3, making its gelation closed to physiological conditions. Owing to its versatile amine chemistry for biological integration and its pH-dependent solubility for film formation, chitosan is an ideal candidate for broad biological and biomedical applications. Over the last 2 decades, depositing chitosan on the cathode surface via electrical signals has been widely explored by imposing a high pH gradient around the cathode with water electrolysis to induce structure formation.[10,30–37] The cathodic neutralization prompts direct electron transfer to the amine groups of chitosan chains and deposits a hydrogel or membrane layer on the electrode surfaces. Therefore, chitosan electrodeposition presents an integrating and communicating interface between electronic devices and biological entities with unique spatiotemporal programmability.[10,31,32,36–38] Several challenges, however, remain in fabricating chitosan membrane structures with electrodeposition. First, the electrodeposition on the electrode surface is not suitable to fabricate standalone membranes that allow for fluidic access to both sides of the structure for broader applications. Second, the mass production of chitosan membranes with electrodeposition is difficult due to the need for at least one working electrode for each film. Finally, the fabricated films are difficult to harvest and repackage for further usage, and the films may be contaminated with metallic ions if inert electrodes of precious metals are not used.[39] Recently, standalone membrane structures have been assembled with flows in microchannels by hydroxide ions diffusing from a nearby basic buffer solution.[40–45] Nevertheless, the flow-assembled method remains not scalable due to its technical complexity.

Here, we report an innovation of electrofabricating freestanding chitosan membranes at the interface of polyelectrolytes without electrodes at the fabrication site, which dramatically differs from the widely explored electrodeposition of chitosan films on electrode surfaces. Furthermore, we demonstrated that the instantaneous flow of hydroxyl ions in the alginate solution, instead of the slower migration of pH gradients as in the electrodeposition of chitosan on the cathode surfaces, is responsible for growing the freestanding membrane structure in the electrolyte with distal electrodes. The presented interfacial electrofabrication can be expanded to the interface of other materials and presents a new direction in using electrical signals for manufacturing.

RESULTS AND DISCUSSION

Electrofabrication of Freestanding Chitosan Membrane.

The interfacial electrofabrication was first demonstrated in poly(dimethylsiloxane) (PDMS) microchannels schematically shown in Figure 1a. After the air bubble trapped inside the aperture was extracted out of the PDMS microchannel, the positively charged chitosan and negatively charged alginate chains came into contact electrostatically and formed a polyelectrolyte complex membrane (PECM) at the interface between the two solutions as reported prveviously.[41,42] When a constant direct current was applied through the distal electrodes, the positively charged chitosan chains in the applied electrical field migrated toward the cathode, which was similar to gel electrophoresis. Since the chitosan and alginate biopolymer chains were too large to cross the PECM, they were stopped at

the PECM. Chitosan chains were then deprotonated by hydroxyl ions from the alginate side and solidified as a membrane structure (Figure 1b,c), while alginate chains, with a pK_a value in the range of 3.4–4.4, remained intact. As the origin of chitosan membrane growth in interfacial electrofabrication, the PECM was formed in a spontaneous, flexible, and controlled manner, which offers boundless potential for applications in bioelectronics, biomedical field, and more.

The sequence of the interfacial electrofabrication in microfluidics between chitosan (0.5% w/v, pH 5.3) and alginate (0.5% w/v, pH 6) solutions at 60 A/m^2 applied current density is shown in Figure 1d. These sequential images show: (i) the trapping of an air bubble in the PDMS microchannel, (ii) the vacuuming of the air bubble out of the microchannel network, (iii) the formation of the PECM, (iv) the growth of the chitosan membrane on the PECM to 30 μm thick in 5 min, and (v) the final membrane at 56 μm thick in 10 min. A similar sequence of the electrofabrication process is shown in the Supporting Video S1. Many experimental parameters may affect the interfacial electrofabrication of chitosan membranes. These parameters include but are not limited to the applied current density, the current connection time, the pH and concentration of chitosan and alginate solutions, and additional components such as chloride and sodium ions in the chitosan solution. In this report, three key parameters including (i) fabrication time, (ii) current density, and (iii) the pH level of alginate solution were characterized while the pH of chitosan remained at 5.3.

Figure 2a,b shows the time-dependent growth of the membrane thickness and volume, respectively, as functions of current density (40, 60, and 80 A/m^2) and pH of alginate solution (pH 6, 8, and 10). These results clearly show that: (1) the higher the applied current density, the faster the membrane grew as shown within each panel; (2) the higher the pH of alginate solution, the faster the membrane grew as shown in the panels from left to right; (3) the growth curves of the membrane thickness in Figure 2a were nonlinear in the first 3 min, presumably due to the irregular membrane shape from inside the aperture into the microchannel; but importantly, (4) the growth curves of the membrane volume (membrane area times channel height) were almost linear throughout the 10 min. In particular, for the case of pH 8 alginate solution (middle panel of Figure 2b), the volume growth rates, represented by the slopes of line fits of the curves, were 41.3, 62.5, and 82.3 × 10^3 μm^3/min for the current density of 40, 60, and 80 A/m^2, respectively. Theoretically, chitosan chains of similar molecular weight in a constant electric filed should migrate at a similar rate, which explains the almost linear growth curves of the membrane volume over time. These results demonstrate that the interfacial electrofabrication is programmable with current density, solution pH, and time, and the process is simple and robust.

The demonstrated capability to form chitosan membranes in the middle of microchannels without the need for electrodes at the fabrication site is novel and potentially important. First, the location of the chitosan membrane was defined by the location of the PECM, which is flexible and controllable by device design and process manipulation. Second, the size, type, and location of electrodes are no longer important. In a microdevice integrated with electrodes, the electrode fabrication is normally the major portion of the cost. Here, *ex situ*, simple and exchangeable electrodes could be repeatedly used with the disposable, cheap PDMS devices. Third, the freestanding configuration of the fabricated chitosan

membrane offers easy fluidic and electrical access to both sides of the membrane, which may be of importance in a myriad of filtration, sampling, and sensing applications in chemical, biochemical, and potential battery engineering.

Visualization of Chitosan Chains' Migration.

To visualize the migration and deposition of chitosan chains onto the PECM, green fluorescent polystyrene beads of 200 nm in diameter were mixed in chitosan solution at the concentration of 0.2 mg/mL. The electrofabrication of the chitosan-beads mixture at 60 A/m^2 current density for 10 min is shown in Figure 3a and Supporting Video S2. In a recent report about flow-assembly of chitosan membrane with polystyrene beads, the noncharged beads trapped in chitosan chains moved along with chitosan chains to form highly aligned chitosan–polystyrene composite membranes.[46] Here, it was clearly observed that electrically neutral fluorescent particles were taken along by the entangling chitosan chains and packed in the chitosan membrane on the PECM (Supporting Video S2). The fluorescence intensities over time through a fixed section of the membrane was analyzed and plotted in Figure 3b, which shows that the locations of entrapped particles did not change over time, and speed of the moving particles before reaching the fabricated chitosan membrane was not obviously slowed down. The size of fluorescent spots was not uniform because of bead aggregation. When the applied current was off, chitosan solution could be easily washed away while the fabricated chitosan membrane with entrapped fluorescent particles remained intact.

In a control experiment under the same condition except that the fluorescent beads were mixed in alginate solution, as shown in Figure 3c and Supporting Video S3, the fluorescent beads were initially taken along by the entangling alginate chains and accumulated near the PECM, then the tracking speed was slowed down quickly. When the applied current was off, the accumulated fluorescent beads were released back to the original uniform distribution. This was different from the chitosan side where the beads were fixed in the gel even after the current was off. Apparently, the negatively charged alginate chains were attracted toward the anode under the electrical field and were relaxed without gel formation once the electrical force disappeared.

To confirm that the fabricated membrane except the initial PECM layer was chitosan instead of a structure crosslinked with alginate, HCl solution (pH = 3) was used to rinse both sides of the fabricated membrane. It is well known that chitosan is water soluble when the surrounding pH value falls below its pK_a of 6.3, while alginate is insoluble when pH is lower than its pK_a of 3.5. Therefore, if the fabricated membrane contains alginate, it will not be dissolved completely by the acidic solution with a pH lower than 3.5. The results in Figure 3d and Supporting Video S4 clearly show that the membrane except the PECM layer was completely dissolved by mild acidic solution (pH = 3) within minutes, which confirms that the chitosan membrane was fabricated due to neutralization by hydroxyl ions instead of crosslinking by alginate crossed PECM.

Using TrackMate from Fiji,[47] the migration paths of fluorescent particles in Figure 3b were analyzed and plotted as shown in Figure 3e, which interestingly depicts the virtual electric field lines. The local tracking paths in every minute are shown in Supporting Video S5. In comparison, no or minimum particle migration was observed in a control experiment where

chitosan was removed from the solution, which confirms that the particle movement in the chitosan solution was truly a proxy for the chitosan chain migration. The overall motion paths were not symmetric but were originated from the lower left corner in the chitosan channel, where the anode was inserted. The migration paths in Figure 3e, in combination with the velocities of individual fluorescent particles throughout 10 min (blue dots in Figure 3f), depict that: (1) the average velocity of the chitosan chain movement was nearly constant at a rate of about 2 μm/s throughout the deposition process (red curve in Figure 3f); and (2) the number of tracking particles within the viewing region increased almost linearly (blue curve in Figure 3g), which is consistent with the linear growth of membrane volume in Figure 2b. Furthermore, the average fluorescence intensities of the chitosan membrane and the chitosan solution remained the same at 170 and 40, respectively, in arbitrary unit (a.u.) throughout the fabrication process, while the background fluorescent signal was 32. Based on absolute fluorescence signals, it was estimated that the number of fluorescent particles in the chitosan membrane was about 17 times of that in the chitosan solution (0.5% (w/v)). Therefore, the electrofabricated chitosan membrane at the current density of 60 A/m^2 presumably contained about 8.5% (w/v) chitosan.

Mechanism for Membrane Growth during Electrofabrication.

Chitosan electrodeposition on cathode surfaces has been widely explored in the last 2 decades,[10,30–38] and the high pH gradient induced by water electrolysis around the cathode was believed to be the underlying mechanism for the chitosan film formation.[30,32,36] To determine whether the instantaneous flow of hydroxyl ions in the alginate solution or the slow propagation of pH gradients from the cathode surface was responsible for the freestanding membrane growth, the interfacial electrofabrication experiment was repeated in open space with two separate pH indicators: phenol red indicating yellow to red colors for pH 6.8–8.2, and xylenol blue indicating yellow to blue colors for pH 8.0–9.6. The choice to repeat the electrofabrication in open space also helps to demonstrate that the electrofabrication is not limited to be inside microchannels and has the potential to be scaled up. The colors of phenol red at the 0, 3, and 5 min time points during the fabrication process, and at the 6 min time point right after the current disconnection, are shown in Figure 4c(i–iv). Figure 4c(v,vi) shows a refocused view of the membrane and its corresponding three-dimensional (3D) surface plot with ImageJ. Figure 4c(vii,viii) shows the RGB spectra and the corresponding pH profile of the selected rectangular segment in Figure 4c(v). Together, these results confirm that the chitosan membrane started to grow as soon as the electrical current was applied. This happened before the arrival of the high pH gradient from the water electrolysis around the cathode, which is shown as in red color (pH ≥ 8.2) in the lower right corners of (iii)–(vi). Similarly, Figure 4d(i–vii) shows the colors and the RGB spectra of xylenol blue during or right after electrofabrication, while Figure 4d(viii) shows the corresponding pH profile corresponding to Figure 4d(v,vi). Importantly, although the lower and higher bounds of the pH profiles are different due to the different color spectrum limits of the pH indicators, the pH profile humps around the chitosan membrane have the similar maximum values of pH 8.21 in Figure 4c(viii) and pH 8.28 in Figure 4d(viii). Together, these results further confirm that the growth of chitosan membrane was due to the immediate flow of hydroxyl ions from the nearby alginate solution right upon applying

electrical signal, rather than the slow migration of the high pH gradient from the cathode surface.

pH Change in Membrane and Interpretation.

It is interesting to note that Figure 4c(iii),4d(iii) shows pink and blue boundaries, respectively, near the chitosan side, which quickly diffused back to the membranes upon current disconnection. To better visualize and understand this phenomenon, the electrofabrication with phenol red was performed again in microchannels at 40 A/m^2 current density. The molecular structure and color transition of phenol red depending on pH are schematically shown in Figure 5a. Figure 5b and Supporting Video S9 show the sequential color changes of phenol red during and right after electrofabrication. It was clearly observed that a pink boundary moved along with the membrane growth front toward the chitosan solution but, remarkably, leaving no color inside the chitosan membrane (Figure 5b(iii,iv)). Once the current was disconnected, the obvious pink boundary quickly diffused back into the chitosan membrane, while a weaker pink boundary on the alginate side also diffused into the membrane (Figure 5b(v)). One minute after the current disconnection, the color in the whole membrane reached equilibrium (Figure 5b(vi)). The corresponding pH profiles at 0 min, 20 s, and 8 min when the current was ON, and 9 min when the current was OFF, are plotted in Figure 5c. The dash segment in Figure 5c(iii) indicates the interpreted pH level in the membrane with no color, as shown in Figure 5b(iii,iv).

Upon carefully examining the relationship between the molecular structural change and the color transition of phenol red in Figure 5a, a plausible explanation of the no color region in the membrane is proposed and schematically shown in Figure 5d. At the onset of electrofabrication, hydroxyl ions preexisting in the alginate polyelectrolyte fluxed to the PECM (Figure 5d(ii)), which deprotonated the amine groups on chitosan chains with a pK_a of 6.3

$$\left[-NH_3^+\right] + [OH^-] \rightleftharpoons [-NH_2] + H_2O \quad (1)$$

Excessive hydroxyl ions also deprotonated the phenol red with a pK_a of 7.7[48]

$$[HPS^-] + [OH^-] \rightleftharpoons \left[PS^{2-}\right] + H_2O \quad (2)$$

Meanwhile, OH^- ions were replenished with the water hydrolysis at the cathode and started to migrate toward the membrane formation site at the electrolyte interface. As the chitosan membrane grew, however, the local accumulation of OH^- ions exceeded the depletion of positively charged amine groups on chitosan, resulting in higher pH inside the membrane than the surrounding electrolyte solution. The excessive accumulation of OH^- ions inside the chitosan membrane potentially acted as a high energy barrier that repelled the PS^{2-} ions to the membrane growth front and restricted the HPS^- ions in the alginate side from diffusing into the membrane (Figure 5d(iii)). Because PS^{2-} were more negatively charged than HPS^-, more PS^{2-} ions were accumulated at the membrane growth front than the amount of HPS^- ions were trapped at the PECM side. When the current was disconnected

and the energy barrier in the membrane disappeared, the phenol red molecules diffused back into the membrane. Apparently, the higher amount of PS^{2-} ions at the membrane growth front diffused into the membrane at a higher rate than the relatively lower amount of HPS^{-} ions diffusing from the PECM side (Figure 5b(v)). The diffusion of phenol red ions reached equilibrium within 1 min and the red color was uniform throughout the membrane (Figure 5b(vi)). In the following few minutes, the OH^{-} ions continued to diffuse out of the membrane and the red color in the membrane slowly fade away.

In summary, the fact that no color was observed inside the chitosan membrane during the interfacial electrofabrication process was plausibly due to the depletion of the negatively charged phenol red molecules. The pH level inside the chitosan membrane, however, was presumably the same as that at the membrane growth front, which was around 8.28 as shown in Figure 4d(viii) and plotted as a dashed line through the membrane in Figure 5c(iii). This is significant for applications with proteins and other biological entities either embedded inside the chitosan membrane or decorated on the membrane surface—they do not have to experience the high pH gradient environment while the high pH environment is normally unavoidable in surface electrodeposition.

It is worthwhile to point out that the electrofabrication presented here was conducted with constant current densities in the electrolyte. Therefore, the neutralization rate of chitosan chains remained constant, and the membrane volume growth rates were constant as reflected with the almost linear slopes in Figure 2b. While this first report focuses on the membrane growth process under constant current density, the deprotonation and localization of chitosan chains during the interfacial electrofabrication may be further revealed by (1) characterizing the electrofabrication process under constant electrical potential, (2) modeling the ion transport and the molecular chain migration with Nernst–Planck equations, (3) examining how the constant electrical field thus the membrane growth rate might be attenuated by salt compositions of various levels, and (4) investigating the influence of the concentration and molecular weight of chitosan molecules on the interfacial electrofabrication process. These studies in the future should reveal more insight about the mechanisms of interfacial electrofabrication and offer further manipulation for broader applications.

CONCLUSIONS

Using electrical signals to guide material depositions, in processes such as electroplating or electrodeposition, has a long-standing history in metal coating, electronic chip fabrication, and biomaterial coating. These processes fabricate conductive materials or biomaterials directly onto the cathode surface. Here, we demonstrated for the first time a novel interfacial electrofabrication without the need of electrodes on the fabrication site, and the fabrication site was not limited to microchannels as demonstrated in the electrofabrication of larger chitosan membrane in open space.

This novel electrofabrication not only opens a new direction to integrate biology with devices but also has many unique features. First, different from the chitosan membranes electrodeposited on the cathode surface, the location of the chitosan membranes here is defined by where the PECM is formed, which is flexible and controllable by the device

design and the manipulation of the electrolyte solutions. Second, the size and location of the chitosan membranes are no longer limited by the type and size of electrodes, which eases the concern of possible metallic ion contaminations. Third, the fabrication can be further manipulated with simple mesh structures that facilitate the formation of the PECM. Fourth, the process may be extended to the fabrication of other polymers and metals at the interfaces of other fluid phases. Finally and most importantly, the freestanding configuration of the fabricated chitosan membranes with easy fluidic and electrical accesses to both sides of the membrane may be of importance in a myriad of filtration, sampling, and sensing applications in chemical, biochemical, and potential battery engineering.

Overall, the reported interfacial electrofabrication presents an unprecedented approach to fabricate membrane structures without the need of on-site electrodes, provides a new direction to integrate biology with devices, and might shift the paradigm of using electrical signals for manufacturing.

EXPERIMENTAL SECTION

Solution Preparation.

The solution of 0.5% w/v chitosan was prepared by dissolving the chitosan flakes (85% deacetylated, medium molecular weight, Sigma-Aldrich) in deionized (DI) water, with 1 mol HCl added dropwise to pH 2 and left by stirring on a stirring plate overnight, followed by two times of filtration and dropwise addition of 1 mol NaOH to adjust its pH to 5.3. Alginate powder (extracted from brown algae, medium viscosity, Sigma-Aldrich) was dissolved in DI water at a concentration of 0.5% w/w and followed by stirring on a stirring plate overnight, then dropwise addition of 1 mol NaOH to adjust its pH. The pH of the alginate solution was tuned dropwise with 1 mol NaOH or HCl solutions to be 6.0, 8.0, or 10.0 for the experiments in Figure 2, 6.4 for experiments in Figure 5, and 6.0 for the rest of all other experiments. Green fluorescent polystyrene beads of 200 nm in diameter (1 mL of 1% solid suspensions (10 mg/mL) in DI water, Degradex) were suspended in the chitosan and alginate solutions, respectively, at a concentration of 0.2 mg/mL. Phenol red indicator (ACS grade, Fisher Scientific) and xylenol blue indicator (indicator grade, Sigma-Aldrich) were dissolved in both chitosan and alginate solutions at its maximum solubility 0.77 and 0.2 mg/mL, respectively.

Interfacial Electrofabrication in Microfluidic Devices.

The PDMS microchannels were fabricated using the routine soft lithography technique and bounded with oxygen plasma to glass slides as previously reported.[42,44,49] An aperture of 50 μm in width and height was connected to two 50-μm-deep and 500-μm-wide channels. Two metal couplers (22ga × 8 mm, Instech Laboratories, Inc.), functioning as both capillary connectors and distal electrodes, were inserted into one terminal of each channel, while the other terminals of the channels were left open. After chitosan and alginate solutions were pumped into the microchannels by syringe pumps (NE-1000, New Era Pump Systems, Inc.) at 1 μL/min, an air bubble was naturally trapped in the aperture between the two solutions due to the hydrophobicity of PDMS (Figure 1d(i)). The pumps were stopped, and the air bubble was then vacuumed out of the gas permeable PDMS device

with an add-on vacuuming chamber as previously reported.[41] A polyelectrolyte complex membrane (PECM) was spontaneously formed within the aperture, where the positively charged chitosan and negatively charged alginate solutions came into contact.[42] When a direct current of 40, 60, or 80 A/m^2 from a power supply (Keithley 2280S-32–6, Keithley Instruments) was applied through the distal electrodes, a chitosan membrane was fabricated on PECM between the chitosan (0.5% w/v, pH 5.3) and the alginate (0.5% w/v) solutions. All membranes in microchannels were electrofabricated within 10 min while the flows were stopped, and manually rinsed with PBS. The dissolving of electrofabricated chitosan membrane in Figure 2d was performed by pumping the HCl solution (pH = 3) at 5 μL/min.

Interfacial Electrofabrication in Open Space.

To generalize the interfacial electrofabrication without the need of on-site electrodes, experiments in open space were carried out with chitosan and alginate solution drops placed side by side on a glass slide on the microscope stage. Two metal electrodes were immerged in the solution drops away from the solution interface (Figure 4a(i,ii)), while the growth of the chitosan membrane was recorded under a microscope with a 4× objective. Upon applying a direct current of 1 mA (unspecified current density due to the undetermined area of the electrolyte interface), a chitosan membrane started to form at the PECM interface, while electrolytic gas bubbles were visible on the electrodes (Figure 4b(i)). Supporting Video S6 records the electrofabrication, while Figure 4b(ii) shows the zoom-in view of the chitosan membrane grown in 3 min to about 0.6 mm thick.

Interfacial Electrofabrication with pH Indicators.

The electrofabrication in open space was further monitored with pH indicators mixed in both chitosan and alginate solutions to reveal the real-time pH change around the fabrication site during electrofabrication (Supporting Videos S7 and S8). Two pH indicators were used in separate experiments: phenol red of 0.77 mg/mL, indicating yellow to red colors from pH 6.8 to 8.2, and xylenol blue of 0.2 mg/mL, indicating yellow to blue colors from pH 8.0 to 9.6. The pH levels of the chitosan and alginate solutions were adjusted to 5.3 and 6.0, respectively, for both indicators. To further examine the pH change inside the chitosan membrane, interfacial electrofabrication with phenol red in both chitosan (pH = 5.3) and alginate (pH = 6.0) solutions was performed in microchannels at a current density of 40 A/m^2 and recorded under a microscope.

Microscopy and Data Analysis.

Bright-field and fluorescent images were taken with a Ludesco EXI-310 inverted microscope, except that Figure 4a(i),b(i) was taken using a iPhone X and Figure 5b was taken with a Zeiss Axio Observer Z1 inverted microscope. ImageJ with the Fiji image processing package (NIH) was used for image processing and the following data analysis. The thickness and area of membranes were measured against a calibration dimension, then the volume of membranes was calculated by multiplying the area of membranes with the thickness of microchannel (50 μm). The tracking of fluorescent particles in the electrofabrication process was analyzed using TrackMate in Fiji to plot the tracked paths and extract the particles tracking data including velocity and spots count. The fluorescent intensity profiles through the membranes were plotted with Fiji. The average fluorescent

intensities of the whole membrane, the chitosan channel with fluorescent beads, and the alginate channel without fluorescent beads as background were quantified at every minute time point. The color of both pH indicators phenol red and xylenol blue inside microchannels (height: 50 μm) and in open space (height: about 1 mm) was calibrated with fixed pH buffer as reference for pH interpretation. The color of images was analyzed and plotted in RGB value for better comparison. The 3D surface plots of phenol red and xylenol blue were generated with Fiji.

Supplementary Material

Refer to Web version on PubMed Central for supplementary material.

ACKNOWLEDGMENTS

The authors would like to thank Dr. Chuan-Fu Lin and Mireille Muhoza for their valuable comments on the manuscript, and Jabez J. Luo for proofreading.

Funding

This work was funded by the National Science Foundation (CAREER #1553330), the National Institute of Health (1R15GM129766-01), and the School of Engineering at the Catholic University of America.

REFERENCES

(1). Chen X; Shen JReview of membranes in microfluidics. J. Chem. Technol. Biotechnol. 2017, 92, 271–282.

(2). Koev ST; Powers MA; Yi H; Wu L-Q; Bentley WE; Rubloff GW; Payne GF; Ghodssi RMechano-transduction of DNA hybridization and dopamine oxidation through electrodeposited chitosan network. Lab Chip2007, 7, 103–111. [PubMed: 17180212]

(3). Tan X; Rodrigue DA Review on Porous Polymeric Membrane Preparation. Part I: Production Techniques with Polysulfone and Poly(Vinylidene Fluoride). Polymers2019, 11, No. 1160.

(4). Tasselli F; Jansen J; Drioli EPEEKWC ultrafiltration hollowfiber membranes: Preparation, morphology, and transport properties. J. Appl. Polym. Sci. 2004, 91, 841–853.

(5). Remanan S; Sharma M; Bose S; Das NCRecent advances in preparation of porous polymeric membranes by unique techniques and mitigation of fouling through surface modification. ChemistrySelect2018, 3, 609–633.

(6). Guillen GR; Pan Y; Li M; Hoek EMPreparation and characterization of membranes formed by nonsolvent induced phase separation: a review. Ind. Eng. Chem. Res. 2011, 50, 3798–3817.

(7). Kazek-Kęsik A; Krok-Borkowicz M; Dercz G; Donesz-Sikorska A; Pamuła E; Simka WMultilayer coatings formed on titanium alloy surfaces by plasma electrolytic oxidation-electrophoretic deposition methods. Electrochim. Acta2016, 204, 294–306.

(8). Boccaccini A; Keim S; Ma R; Li Y; Zhitomirsky IElectrophoretic deposition of biomaterials. J. R. Soc. Interface2010, 7, S581–S613. [PubMed: 20504802]

(9). Schwarzacher WElectrodeposition: a technology for the future. Electrochem. Soc. Interface2006, 15, 32–33.

(10). Li J; Wu S; Kim E; Yan K; Liu H; Liu C; Dong H; Qu X; Shi X; Shen J; et al.Electrobiofabrication: electrically based fabrication with biologically derived materials. Biofabrication2019, 11, No. 032002.

(11). Jayakrishnan DSElectrodeposition: The Versatile Technique for Nanomaterials. In Corrosion Protection and Control Using Nanomaterials; Elsevier, 2012; pp 86–125.

(12). Schwartz DElectrodeposition and Nanobiosystems; Electrochemical Society Inc.: Pennington, NJ, 2006.

(13). Xu W; Fu K; Bohn PWElectrochromic sensor for multiplex detection of metabolites enabled by closed bipolar electrode coupling. ACS Sens. 2017, 2, 1020–1026. [PubMed: 28750540]

(14). Walker G; Ramsey J; Cavin R III; Herr D; Merzbacher C; Zhirnov VA Framework for Bioelectronics: Discovery and Innovation; National Institute of Standards and Technology, 2009.

(15). Agarwala S; Lee JM; Ng WL; Layani M; Yeong WY; Magdassi SA novel 3D bioprinted flexible and biocompatible hydrogel bioelectronic platform. Biosens. Bioelectron. 2018, 102, 365–371. [PubMed: 29172145]

(16). Hsiao Y-S; Ho B-C; Yan H-X; Kuo C-W; Chueh D-Y; Yu H.-h.; Chen PIntegrated 3D conducting polymer-based bioelectronics for capture and release of circulating tumor cells. J. Mater. Chem. B2015, 3, 5103–5110. [PubMed: 32262462]

(17). Katz EImplantable Bioelectronics—Editorial Introduction. In Implantable Bioelectronics; Wiley: Weinheim, 2014.

(18). Prakash S; Chakrabarty T; Singh AK; Shahi VKPolymer thin films embedded with metal nanoparticles for electrochemical biosensors applications. Biosens. Bioelectron. 2013, 41, 43–53. [PubMed: 23083910]

(19). Simon D; Ware T; Marcotte R; Lund BR; Smith DW; Di Prima M; Rennaker RL; Voit WA comparison of polymer substrates for photolithographic processing of flexible bioelectronics. Biomed. Microdevices2013, 15, 925–939. [PubMed: 23852172]

(20). Willner I; Baron R; Willner BIntegrated nanoparticle–biomolecule systems for biosensing and bioelectronics. Biosens. Bioelectron. 2007, 22, 1841–1852. [PubMed: 17071070]

(21). Svennersten K; Larsson KC; Berggren M; Richter-Dahlfors AOrganic bioelectronics in nanomedicine. Biochim. Biophys. Acta2011, 1810, 276–285. [PubMed: 20933573]

(22). Berggren M; Richter-Dahlfors AOrganic bioelectronics. Adv. Mater. 2007, 19, 3201–3213.

(23). Yuk H; Lu B; Zhao XHydrogel bioelectronics. Chem. Soc. Rev. 2019, 48, 1642–1667. [PubMed: 30474663]

(24). Zhang A; Lieber CMNano-bioelectronics. Chem. Rev. 2016, 116, 215–257. [PubMed: 26691648]

(25). Bhattarai N; Gunn J; Zhang MChitosan-based hydrogels for controlled, localized drug delivery. Adv. Drug Delivery Rev. 2010, 62, 83–99.

(26). Croisier F; Jérôme CChitosan-based biomaterials for tissue engineering. Eur. Polym. J. 2013, 49, 780–792.

(27). Koev S; Dykstra P; Luo X; Rubloff G; Bentley W; Payne G; Ghodssi RChitosan: an integrative biomaterial for lab-on-a-chip devices. Lab Chip2010, 10, 3026–3042. [PubMed: 20877781]

(28). Suginta W; Khunkaewla P; Schulte AElectrochemical biosensor applications of polysaccharides chitin and chitosan. Chem. Rev. 2013, 113, 5458–5479. [PubMed: 23557137]

(29). Rafique A; Zia KM; Zuber M; Tabasum S; Rehman SChitosan functionalized poly (vinyl alcohol) for prospects biomedical and industrial applications: A review. Int. J. Biol. Macromol. 2016, 87, 141–154. [PubMed: 26893051]

(30). Wu L-Q; Gadre AP; Yi H; Kastantin MJ; Rubloff GW; Bentley WE; Payne GF; Ghodssi RVoltage-dependent assembly of the polysaccharide chitosan onto an electrode surface. Langmuir2002, 18, 8620–8625.

(31). Wu S; Yan K; Li J; Huynh RN; Raub CB; Shen J; Shi X; Payne GFElectrical cuing of chitosan's mesoscale organization. React. Funct. Polym. 2020, 148, No. 104492.

(32). Yi H; Wu L-Q; Bentley WE; Ghodssi R; Rubloff GW; Culver JN; Payne GFBiofabrication with chitosan. Biomacromolecules2005, 6, 2881–2894. [PubMed: 16283704]

(33). Pang X; Zhitomirsky IElectrodeposition of composite hydroxyapatite–chitosan films. Mater. Chem. Phys. 2005, 94, 245–251.

(34). Fusco S; Chatzipirpiridis G; Sivaraman KM; Ergeneman O; Nelson BJ; Pané SChitosan electrodeposition for microrobotic drug delivery. Adv. Healthcare Mater. 2013, 2, 1037–1044.

(35). Cheng Y; Gray KM; David L; Royaud I; Payne GF; Rubloff GWCharacterization of the cathodic electrodeposition of semicrystalline chitosan hydrogel. Mater. Lett. 2012, 87, 97–100.

(36). Cheng Y; Luo X; Betz J; Buckhout-White S; Bekdash O; Payne GF; Bentley WE; Rubloff GWIn situ quantitative visualization and characterization of chitosan electrodeposition with paired sidewall electrodes. Soft Matter2010, 6, 3177–3183.

(37). Kim E; Xiong Y; Cheng Y; Wu H-C; Liu Y; Morrow BH; Ben-Yoav H; Ghodssi R; Rubloff GW; Shen J; et al.Chitosan to connect biology to electronics: Fabricating the bio-device interface and communicating across this interface. Polymers2015, 7, 1–46.

(38). Tsai C; Payne GF; Shen JExploring pH-responsive, switchable crosslinking mechanisms for programming reconfigurable hydrogels based on aminopolysaccharides. Chem. Mater. 2018, 30, 8597–8605.

(39). Dharmadasa I; Haigh JStrengths and advantages of electrodeposition as a semiconductor growth technique for applications in macroelectronic devices. J. Electrochem. Soc. 2006, 153, G47–G52.

(40). Hu P; Raub CB; Choy JS; Luo XModulating the properties of flow-assembled chitosan membranes in microfluidics with glutaraldehyde crosslinking. J. Mater. Chem. B2020, 8, 2519–2529. [PubMed: 32124900]

(41). Pham P; Vo T; Luo XSteering air bubbles with an add-on vacuum layer for biopolymer membrane biofabrication in PDMS microfluidics. Lab Chip2017, 17, 248–255. [PubMed: 27942655]

(42). Luo X; Wu H-C; Betz J; Rubloff GW; Bentley WEAir bubble-initiated biofabrication of freestanding, semi-permeable biopolymer membranes in PDMS microfluidics. Biochem. Eng. J. 2014, 89, 2–9.

(43). Luo X; Wu H-C; Tsao C-Y; Cheng Y; Betz J; Payne GF; Rubloff GW; Bentley WEBiofabrication of stratified biofilm mimics for observation and control of bacterial signaling. Biomaterials2012, 33, 5136–5143. [PubMed: 22507453]

(44). Luo X; Berlin DL; Betz J; Payne GF; Bentley WE; Rubloff GWIn situ generation of pH gradients in microfluidic devices for biofabrication of freestanding, semi-permeable chitosan membranes. Lab Chip2010, 10, 59–65. [PubMed: 20024051]

(45). Gu Y; Hegde V; Bishop KJMeasurement and mitigation of free convection in microfluidic gradient generators. Lab Chip2018, 18, 3371–3378. [PubMed: 30256366]

(46). Ly KL; Raub CB; Luo XTuning the porosity of biofabricated chitosan membranes in microfluidics with co-assembled nanoparticles as templates. Mater. Adv. 2020, 1, 34–44. [PubMed: 33073238]

(47). Tinevez J-Y; Perry N; Schindelin J; Hoopes GM; Reynolds GD; Laplantine E; Bednarek SY; Shorte SL; Eliceiri KWTrackMate: An open and extensible platform for single-particle tracking. Methods2017, 115, 80–90. [PubMed: 27713081]

(48). Tamura Z; Maeda MDifferences between phthaleins and sulfonphthaleins. J. Pharm. Soc. Jpn. 1997, 117, 764–770.

(49). Li K; Correa S; Pham P; Raub C; Luo XBirefringence of flow-assembled chitosan membranes in microfluidics. Biofabrication2017, 9, No. 034101.

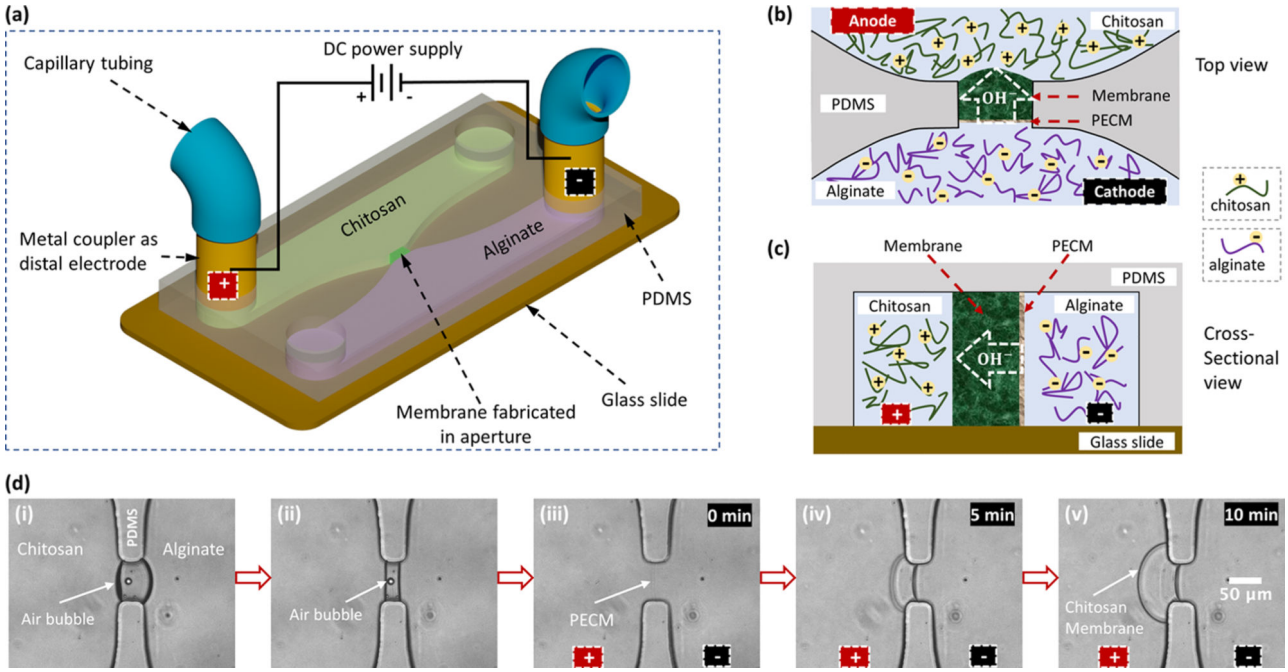

Figure 1.

Interfacial electrofabrication of a chitosan membrane in poly(dimethylsiloxane) (PDMS) microchannels with distal electrodes. (a) Schematic of the electrofabrication across an aperture between two microchannels containing positively charge chitosan (green) and negatively charged alginate (purple) solutions. The two metal couplers at the channel terminals function as both capillary connectors and distal electrodes. (b, c) Schematic top and cross-sectional views of the chitosan membrane growth due to the ion flow from alginate to chitosan solutions. (d) Sequence of the interfacial electrofabrication in microfluidics: (i) an air bubble was naturally trapped inside the aperture due to the hydrophobicity of PDMS; (ii) the air bubble was vacuumed out by an add-on PDMS chamber (not shown); (iii) a polyelectrolyte complex membrane (PECM) was spontaneously formed between chitosan (pH 5.3) and alginate (pH 6); and (iv), (v) the chitosan membrane was grown to 30 and 56 μm thick in 5 and 10 min, respectively, at a current of 60 A/m^2 applied through the distal electrodes.

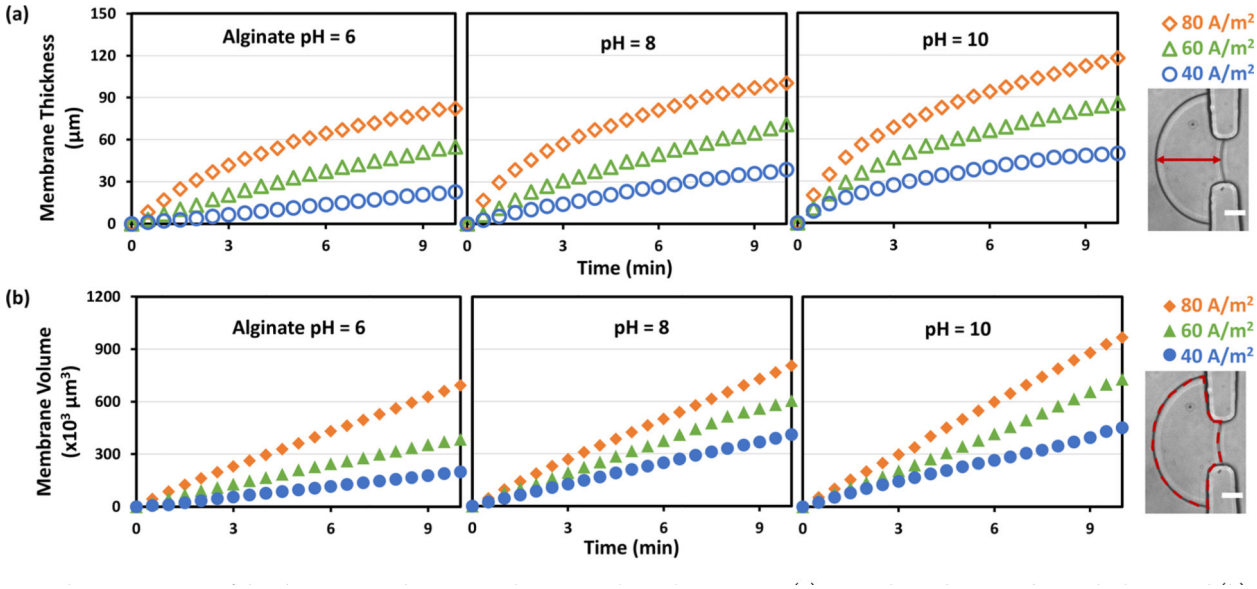

Figure 2.

Characterizations of the chitosan membrane growth in microchannels over time. (a) Time-dependent membrane thickness and (b) time-dependent membrane volume as a function of current density (40, 60, and 80 A/m^2) and pH level (pH 6, 8, 10) of alginate solution. Insets depict the corresponding thickness and volume measurements. Scale bars: 20 μm.

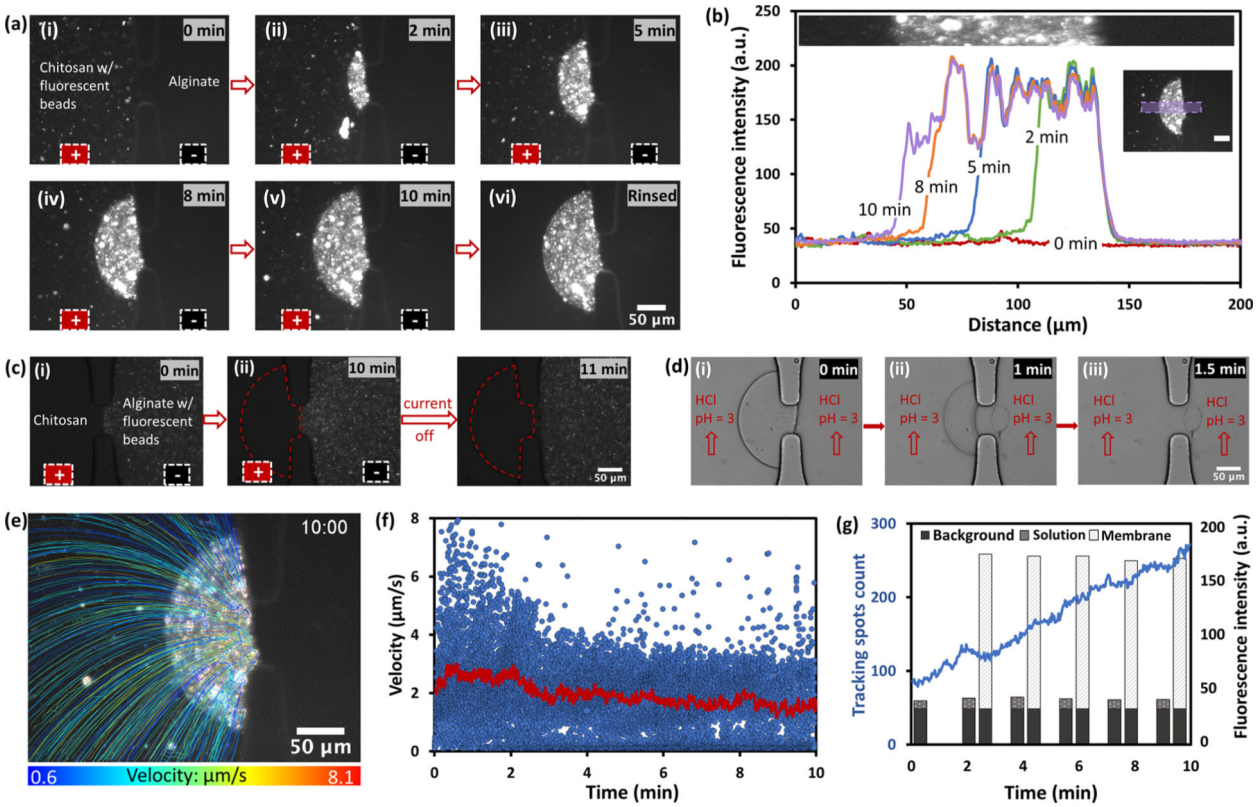

Figure 3.

Visualization of chitosan chain migration during the electrofabrication in microchannels. (a(i)–(v)) Sequence of the codeposition of a chitosan membrane with 200 nm fluorescent beads at 60 A/m^2 over 10 min to visualize the migration and deposition of chitosan chains onto PECM, and (a(vi)) the final deposited chitosan membrane with fluorescent beads after rinsing with phosphate-buffered saline (PBS). (b) Time course profiles of the fluorescence intensity of the deposited membrane with embedded fluorescent beads. Insets correspond to the areas that the fluorescence intensity were plotted. (c) Control experiment under the same condition to visualize the migration of alginate chains (i)–(iii) during the electrofabrication and (iv) 1 min afterwards. (d) Sequence of the electrofabricated chitosan membrane being dissolved by the flowing HCl solution (pH = 3) except the PECM layer. (e) Map of all tracking paths of fluorescent beads in 10 min, with the paths color coded with the mean velocity of each bead. (f) Velocity of each bead in each time frame (blue markers), and the average velocity of all beads at each time frame (red curve). (g) Count of tracking spots in 10 min (blue line) with the average fluorescence intensity of background (black), chitosan solution (meshed), and chitosan membrane (slashed) with fluorescent beads. Scale bars are 20 μm when not specified.

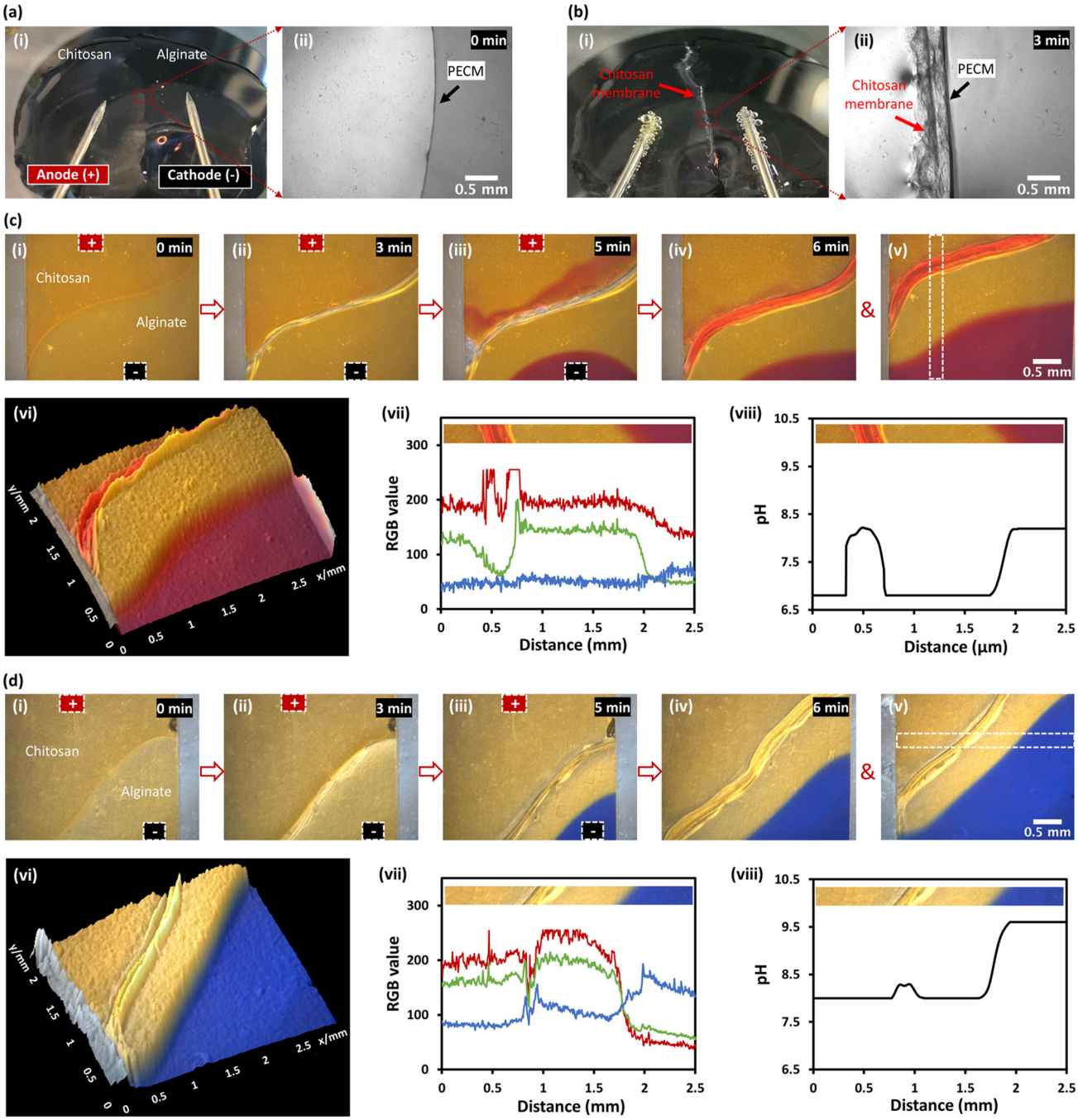

Figure 4.

Electrofabrication in open space with distal electrodes and *in situ* visualization of pH profiles around the fabrication site. (a(i)) Before electrofabrication, chitosan and alginate solution drops were placed side by side on a glass slide on the microscope stage with two immerged electrodes away from the solution interface; (a(ii)) Zoom-in view of the PECM interface between solutions. (b(i)) After applying 1 mA current for 3 min, a chitosan membrane was grown along PECM, and electrolytic gas bubbles were visible on the electrodes; (b(ii)) Zoom-in view of the membrane of about 0.6 mm thick along PECM.

(c) Real-time color and pH changes indicated with phenol red around the solution interface during electrofabrication: (i) 0, (ii) 3, and (iii) 5 min during electrofabrication; (iv) right after current disconnection; (v), (vi) refocused view of the fabricated membrane and its corresponding 3D surface plot; (vii), (viii) the RGB spectra and the corresponding pH profile of the insets referring to the selected rectangular segment in (v). (d) Real-time color and pH changes indicated with xylenol blue around the solution interface during electrofabrication.

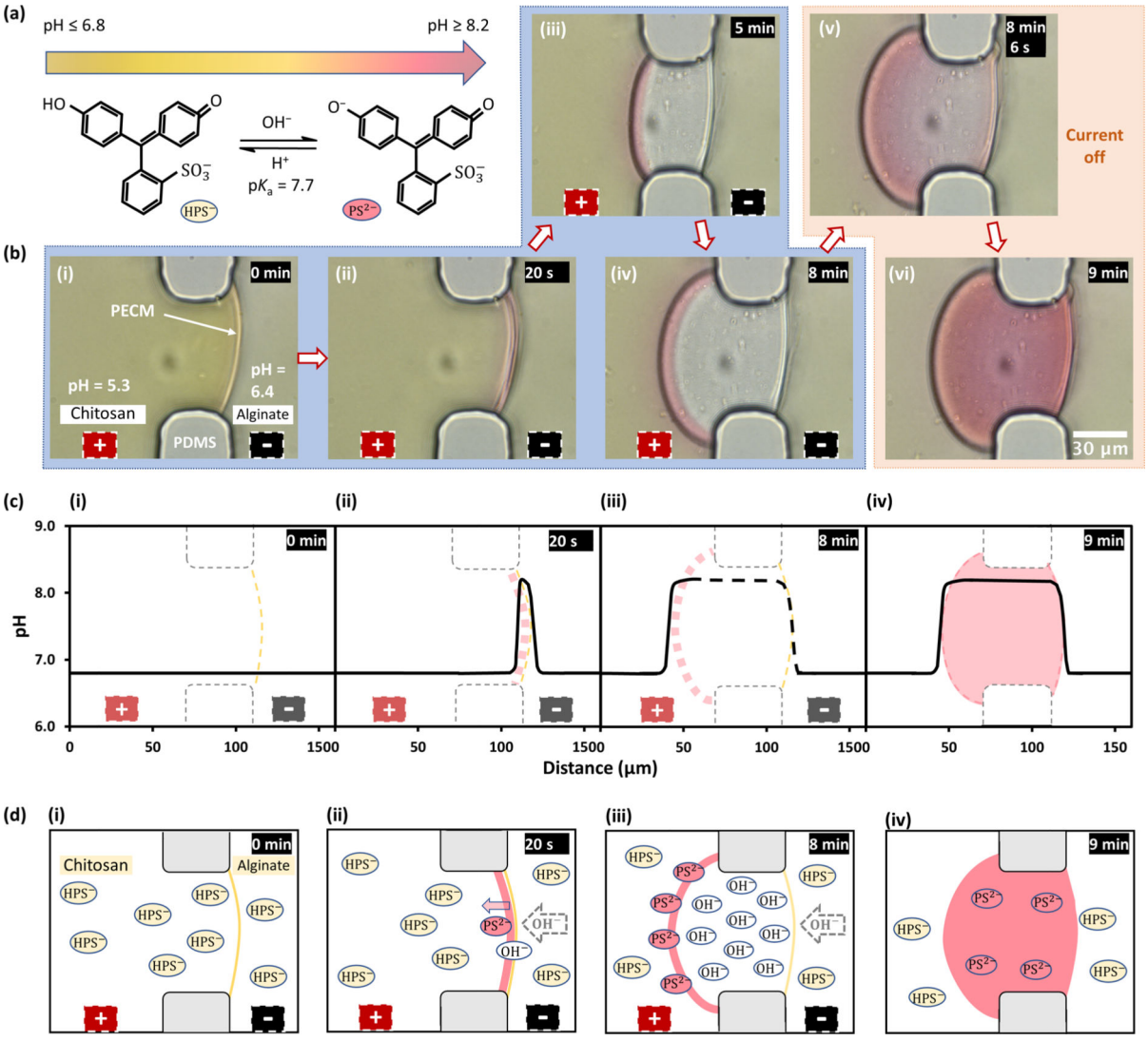

Figure 5.

Color transition and distribution of phenol red, and the corresponding pH profiles across the chitosan membrane during electrofabrication in a microchannel. (a) Transition of phenol red from yellow (pH ≤ 6.8) to red (pH ≥ 8.0) and its structural change from HPS^{-} to PS^{2-}. (b) Color change of phenol red during and after electrofabrication: (i) 0 min, (ii) 20 s, (iii) 5 min, and (iv) 8 min when the current was ON; and (v) 8 min 6 s and (vi) 9 min when current was OFF. (c) pH profiles corresponding to (b) at (i) 0 min, (ii) 20 s, (iii) 8 min when current was ON; and (iv) 9 min when current was OFF. The dash segment of the pH profile in (iii) indicates the interpreted pH level within the membrane, where presumably the phenol red molecules were depleted. (d) Schematic distributions of phenol red molecules across the chitosan membrane during electrofabrication corresponding to (c).